博 士 論 文

Histochemical assessment of the femora of Spontaneously Diabetic Torii-*Lepr*^{fa} (SDT-*fa/fa*) rats that mimic type II diabetes
（Ⅱ型糖尿病モデル Spontaneously Diabetic Torii-*Lepr*^{fa} (SDT-*fa/fa*)ラット大腿骨の組織化学的解析）

令和 7 年 3 月申請

北海道大学

大学院歯学院口腔医学専攻

姚　斉

Abstract

To elucidate the mechanisms underlying diabetic osteoporosis, we conducted a comprehensive histological examination of the femora in Spontaneously Diabetic Torii-*Lepr*^{fa} (SDT-*fa/fa*) rats, an established model for obesity-related type 2 diabetes. Femora from 12 30-week-old male SDT-*fa/fa* rats and age-matched Sprague–Dawley (SD) rats (controls) were used for detailed histochemical analyses, including TRAP, cathepsin K, ALP, PHOSPHO1, DMP-1, MEPE, sclerostin, and osteocalcin staining, as well as silver impregnation, von Kossa staining, and micro-CT imaging. Micro-CT and hematoxylin-eosin staining demonstrated significantly reduced trabecular bone volumes in the femoral metaphyses of SDT-*fa/fa* rats. While the number of TRAP-positive osteoclasts per bone surface (/BS) remained comparable between the two groups, SDT-*fa/fa* rats exhibited reduced areas of ALP-positive osteoblasts/BS and PHOSPHO1-reactive mature osteoblasts/BS. Silver impregnation revealed a well-organized osteocytic lacunar–canalicular system in both groups; however, immunostaining identified aberrant DMP-1 and MEPE expression localized predominantly in lacunae in SDT-*fa/fa* rats, whereas in SD rats, these peptides were evident in both lacunae and canaliculi. Additionally, intense osteocalcin and sclerostin immunoreactivity was detected in osteocytes, along with a higher proportion of osteocalcin-positive osteocytes, in SDT-*fa/fa* rats, distinguishing them from SD controls. In conclusion, SDT-*fa/fa* rats display a notable decline in osteoblastic function and distinctive distribution patterns of osteocyte-derived peptides, suggesting that this diabetic model may manifest alterations in osteoblastic activity and the osteocytic lacunar-canalicular network.

218 words

Key words: ***diabetes, osteoporosis, SDT-fa/fa rat, osteocyte, histochemistry***

Introduction

Diabetes originates from disruptions in glucose metabolism and progresses to multi-organ dysfunction. Type 2 diabetes mellitus (T2DM) is the predominant form of diabetes, contributing substantially to morbidity and mortality due to its prolonged clinical course and the impact of hyperglycemia-induced complications [1]. It is characterized by elevated blood glucose levels, insulin insensitivity from insulin resistance, and impaired insulin secretion [2]. Increasing evidence has underscored a complex relationship between diabetes and osteoporosis: both conditions are metabolic disorders that intersect in multifaceted ways [3]. Patients with T2DM are known to be at higher risk of bone fractures, despite often normal or even increased bone mineral density (BMD) [4, 5], likely due to the development of low-turnover osteoporosis. The reduced bone quality and mechanical properties observed in patients with diabetes have been attributed to impaired bone formation [6-9].

The relationship between fracture risk and BMD in T2DM patients remains under debate. Some studies report that patients with T2DM exhibit an elevated risk of fractures, despite higher BMD at sites such as the femoral neck, shoulders, and spine when assessed via dual-energy X-ray absorptiometry [10]. Others, however, have found lower BMD in T2DM patients with similarly high fracture risk, suggesting that decreased bone strength or additional diabetes-related factors may increase fracture susceptibility [11]. Regardless of BMD, these findings converge on a consensus of heightened fracture risk among individuals with T2DM. With respect to bone turnover, a meta-analysis has demonstrated a marked reduction in bone resorption markers, such as CTX and TRAcP5b, in T2DM patients compared to non-diabetic individuals [12]. A significant limitation, however, lies in the scarcity of histological and histomorphometric studies, which are essential for a more comprehensive understanding of bone turnover and quality in T2DM sufferers.

To address this deficit in bone histology information on T2DM, the Spontaneously Diabetic Torii- *Lepr*^{fa} (SDT-*fa/fa*) rat has been developed as a model of T2DM. These rats were created by introducing the fa allele from the Zucker fatty rat into the SDT-+/+ background [13]. This model displays diabetic complications, including ocular, nephropathic, neuropathic, and osteoporotic manifestations, at an early age [14-19]. Additionally, SDT-*fa/fa* rats have shown reductions in trabecular bone volume, BMD, and mechanical strength in both femur and tibia relative to normal Sprague–Dawley (SD) rats [18].

However, histological analyses of bone turnover and structure in SDT-*fa/fa* rats remain limited. Thus, this study conducted a histochemical examination of the femora of SDT-*fa/fa* rats, aiming to elucidate histological abnormalities associated with T2DM and contribute to a deeper understanding of bone pathology in this diabetic model.

Materials and Methods

Animals and specimen preparation

Thirty-week-old male SDT-*fa/fa* rats and normal Sprague–Dawley (SD) rats (*n* = 12, Japan CLEA, Tokyo, Japan) were handled according to Hokkaido University's guidelines for animal care and research use (approved study protocol #21-0013).

Under anesthesia from an intraperitoneal injection of a combination of anesthetic agents, including 0.3 mg/kg of medetomidine, 4.0 mg/kg of midazolam, and 5.0 mg/kg of butorphanol, blood in right ventricle of the rats was collected using syringes for the measurement of total cholesterol (T-CHO); triglyceride (TG); high-density lipoprotein cholesterol (HDL-C); A hemoglobin A1C (HbA1C); glucose (GLU); blood urea nitrogen (BUN); creatine (CRE); and serum minerals, including calcium (Ca), inorganic phosphate (iP), and so forth, in serum (Oriental Yeast Co., Ltd., Tokyo, Japan). Thereafter, the rats were immediately fixed with 4% paraformaldehyde in a 0.1 M phosphate buffer (pH 7.4) through the left ventricle. Femora were removed and then immersed in the same fixative for 24 h. Right femora were extracted for micro-CT imaging, bone mineral density (BMD) assessment, and von Kossa staining, while left femora were decalcified in a 10% ethylenediaminetetraacetic disodium salt solution for 2 months at 4 °C prior to paraffin embedding. Five µm-thick sagittal sections were cut parallel to the bone longitudinal axis. After histochemical staining (see the following subsections), sections were photographed under a Nikon Eclipse E800 microscope (Nikon Instruments Inc., Tokyo, Japan) using a digital camera (Nikon DXM1200C, Nikon).

Micro-CT analysis

Micro-computed tomography (micro-CT) images of sagittal sections of the right femora from the end of the distal epiphysis to 1.6 cm distally were obtained with a micro-CT system (CosmoScan Fx; Rigaku Corporation, Tokyo, Japan) at a tube voltage of 90 kV and tube current of 88 µA (FOV 25 mm) [20].

Von Kossa staining

Histological sections of epoxy resin-embedded undecalcified specimens obtained from right femora were soaked in an aqueous solution of silver nitrate until a dark brown/black staining of the bone tissue was discernible under a light microscope, as reported in Hasegawa et al. [21].

Immunohistochemistry for cathepsin K, ALP, PHOSPHO1, MEPE, DMP1, sclerostin, and osteocalcin

Dewaxed paraffin sections were immersed in 0.3% H_2O_2 in phosphate-buffered saline (PBS) for 30 min to block endogenous peroxidase activity. To reduce nonspecific binding, 1% bovine serum albumin in PBS (1% BSA-PBS) (Serologicals Proteins Inc., Kankakee, IL) was applied to the sections for 20 min. The sections were then incubated with mouse anti-human cathepsin K antibody (Daiichi Fine Chemical Co., Ltd., Takaoka, Japan) in 1% BSA-PBS at a 1:200 dilution at room temperature for 2 h [20], followed by horseradish peroxidase (HRP)-conjugated anti-mouse IgG (Chemicon International Inc., Temecula, CA) at a 1:100 dilution for 1 h.

For the detection of tissue nonspecific alkaline phosphatase (ALP), phosphoethanolamine /phosphocholine phosphatase 1 (PHOSPHO1), matrix extracellular Phosphoglycoprotein (MEP E), and dentin matrix protein 1 (DMP-1), the sections were incubated with rabbit antisera ag ainst ALP [22], rabbit polyclonal anti-PHOSPHO1 antibody (Cusabio Technology LLC, Houst on, TX) [23], rabbit polyclonal anti-MEPE antibody (Cloud-Clone Corp., Katy, TX) [20], and rabbit anti-DMP-1 antibody (Takara Bio Inc., Otsu, Japan) [24], respectively, in 1% BSA-P BS at dilutions of 1:200 for 1 h at room temperature. Following primary antibody incubatio n, sections were treated with HRP-conjugated goat anti-rabbit IgG (DakoCytomation, Glostru p, Denmark) at a 1:100 dilution for 1 h.

For osteocalcin and sclerostin detection, sections were incubated with goat anti-rat osteocalcin antibody (Biomedical Technologies Inc., St. Stoughton, MA) at a 1:500 dilution [24] and goat anti-mouse sclerostin antibody (R&D Systems Inc., Minneapolis, MN), respectively, at a 1:100 dilution [25], followed by HRP-conjugated anti-goat IgG (American Qualex, San Clemente, CA) at a 1:100 dilution for 1 h.

To visualize all HRP-conjugated immunoreactions, diaminobenzidine tetrahydrochloride was applied as the chromogenic substrate. Finally, all sections were counterstained with methyl green and observed under a light microscope.

Enzyme histochemistry for tartrate-resistant acid phosphatase

Tartrate-resistant acid phosphatase (TRAP) was detected as previously described [20]. Briefly, dewaxed paraffin sections were rinsed with PBS and incubated in a mixture of 2.5 mg of naphthol AS-BI phosphate (Sigma-Aldrich St. Louis, MO), 18 mg of red violet LB salt (Sigma-Aldrich), and 0.76 g of 100 mM L(+) tartaric acid (Nacalai Tesque, Inc., Kyoto, Japan) diluted in 30 ml of a 0.1 M sodium acetate buffer (pH 5.0) for 15 min at 37 °C.

Silver impregnation

To visualize osteocytic canaliculi, dewaxed sections were immersed in a 1% Protargol-S solution

diluted in borax-boric acid (pH 7.4) for 12-48 h at 37°C. After rinsing with distilled water, the reaction was enhanced using an aqueous solution containing 0.2% hydroquinone, 0.2% citric acid, and 0.7% nitric silver. Following additional rinsing, the sections were reduced for 5 min
with a solution of 2.5% anhydrous sodium sulfite, 0.5% potassium bromide, and 0.5% amidol diaminophenol dihydrochloride. They were then treated with 1% gold chloride and subsequently reduced by 2% oxalic acid amidol until black staining of osteocytic canaliculi was visible. After rinsing with distilled water, sections were lightly stained with hematoxylin and eosin.

Quantification of bone volume, histochemical anabolic/catabolic parameters in regions of interest in femoral metaphyses for statistical analyses

To estimate BMD and bone volume per tissue volume (BV/TV) values, we analyzed micro-CT images of the femora, covering the region from the distal end to the longitudinal center. Following our previous report [26], we measured both whole-bone and cancellous bone parameters for whole BMD, whole BV/TV, cancellous BMD, and cancellous BV/TV.

For counts of TRAP-positive osteoclasts per bone surface (N.Oc/BS), as well as for the ALP-positive area per bone surface (ALP+area/BS), and PHOSPHO1-reactive area per bone surface (PHOSPHO1+area/BS), and the percentage of osteocalcin-positive osteocytes, we used rectangular regions of interest (ROIs) measuring 1000 µm in width by 2000 µm in height positioned 200 µm below the horizontal center of the growth plates in sagittal sections of the femora. These ROIs were analyzed with Image-Pro Plus 6.2 (Media Cybernetics, Inc., Bethesda, MD) as described by Hasegawa et al. [27]. Wherever applicable, abbreviations and calculations followed the guidelines of the ASBMR Histomorphometry Nomenclature Committee [28].

Statistical analysis

All differences between the mean values of the two treatments were statistically assessed using Student's *t*-tests, with *P*-values < 0.05 considered significant. All values are presented as means ± SD.

Results

Serum glucose and lipid levels

Serum lipid markers, including total cholesterol (T-CHO); triglycerides (TG); high-density lipoprotein cholesterol (HDL-C); and serum glucose markers, such as glucose (GLU) and HbA1c, were significantly elevated in SDT-*fa/fa* rats, indicating symptoms of both diabetes mellitus and hyperlipidemia **(Table 1)**. In contrast, there were no significant differences in blood urea nitrogen (BUN), creatinine (CRE), and serum calcium (Ca) and inorganic phosphate (iP) concentrations between SD and SDT-*fa/fa* rats.

Histological characteristics of SDT-fa/fa rat femora

Micro-CT and hematoxylin-eosin (H-E) staining images of femora from SD and SDT-*fa/fa* rats revealed reduced cancellous bone in the metaphyseal and epiphyseal regions of SDT-*fa/fa* rats **(Fig. 1A–D)**. Higher magnification images showed a marked decrease in the number and thickness of trabeculae in their metaphyses **(Fig. 1E, F)**. In SDT-*fa/fa* rats, cancellous BMD was significantly reduced, while whole BMD was unaffected, but both whole and cancellous BV/TV were markedly reduced **(Fig. 1G–J)**.

Osteoclast and osteoblast distributions in SD and SDT-fa/fa rats

In both SD and SDT-*fa/fa* rats, TRAP-positive osteoclasts were mainly localized near the chondro–osseous junction in the femoral metaphyses **(Fig. 2A, B)**. TRAP enzyme histochemistry and cathepsin K immunohistochemistry showed numerous osteoclasts of similar size along the trabecular surfaces near this junction **(Fig. 2C–F)**. Statistical analysis revealed no significant difference between the N.Oc/BS values of SD and SDT-*fa/fa* rats **(Fig. 2G)**.

Like osteoclast distribution, ALP-positive osteoblastic cells and PHOSPHO1-reactive mature osteoblasts seemed to be localized relatively close to the chondro–osseous junction in both rat models **(Fig. 3A–D)**. There was no evident difference in bone mineralization, as assessed by von Kossa staining **(Fig. 3E, F)**. However, statistical analysis demonstrated significant reductions in ALP+area/BS and PHOSPHO1+area/BS in the ROI of SDT-*fa/fa* rats when compared with those of SD rats **(Fig. 3G, H)**.

Osteocyte-derived peptide distribution in SD and SDT-fa/fa rats

Silver staining revealed well-organized osteocytic canaliculi within the metaphyseal trabeculae of both SD and SDT-*fa/fa* rats **(Fig. 4A, B)**. Immunoreactivities for DMP-1 and MEPE were detected in the

osteocyte lacunae and canaliculi in SD rats; however, in SDT-*fa/f*a rats, immunoreactivity appeared to be mainly confined to the lacunae, with limited expression in the canaliculi **(Fig. 4C‑F)**. Osteocalcin immunoreactivity was generally observed along the bone surfaces and cement lines in the trabeculae of SD rats, but not in the osteocytic lacunae. Conversely, SDT-*fa/fa* rats exhibited intense osteocalcin immunoreactivity within osteocytic lacunae **(Fig. 4G, H)**. Similarly, sclerostin immunoreactivity appeared more pronounced in the osteocytic lacunae of femora from SDT-*fa/fa* rats than from SD rats **(Fig. 4I, J)**. Statistical analysis further confirmed a significantly greater percentage of osteocalcin-positive osteocytic lacunae in SDT-*fa/fa* rats than in SD rats **(Fig. 4K)**.

Discussion

In this study, we used 30-week-old SDT-*fa/fa* rats, which exhibited bone abnormalities at more advanced stages than those reported by Kimura et al. [18], who observed the onset of diabetic abnormalities in this rat at 16 weeks. While the progression of diabetes is associated with the development of diabetic nephropathy, our 30-week-old SDT-*fa/fa* rats showed no abnormalities in serum calcium and phosphate levels or renal function markers (creatinine and BUN) compared to control SD rats **(See Table 1)**. This suggests that the rats had not developed renal osteodystrophy, specifically chronic kidney disease–mineral and bone disorder, or CKD-MBD. Therefore, our analysis focused on the state of diabetic osteoporosis, specifically in the femoral cancellous bone.

Our histological analysis revealed decreased cancellous BMD and reduced BV/TV in the SDT-*fa/fa* rats, which is consistent with the findings of Kimura et al. [18] and Nomura et al. [29]. Although the number of osteoclasts in the cancellous bone did not change significantly, the lower levels of ALP and PHOSPHO1, both bone formation markers, in the SDT-*fa/fa* rats indicate that the reduction seen in BV/TV is likely due to impaired bone formation rather than increased bone resorption. An interesting observation in our study was the reduced expression of DMP-1 and MEPE in the bone canaliculi of SDT-*fa/fa* rats while osteocalcin accumulation in the lacunae and sclerostin-positive osteocytes increased.

Nomura et al. [29] analyzed the vertebrae (L4, L5) of 8-week-old obese SDT-*fa/fa* rats and SD controls, finding no initial differences in bone morphology. However, at 16 weeks of age, the SDT-*fa/fa* rats exhibited reduced bone volume, BMD, mechanical strength, and osteoblast surface area. Eight weeks of parathyroid hormone (PTH) treatment at a regimen of 60 μg/kg three times per week improved bone volume and osteoblast-related parameters without affecting bone resorption, while treatments with eel calcitonin and risedronate had no effect. This suggests that the decline in bone formation in SDT-*fa/fa* rats is reversible through PTH stimulation, and, as shown by our study, the bone loss is not driven by increased osteoclastic activity.

One notable finding from our study was the altered localization of osteocyte-derived proteins in SDT-*fa/fa* rats compared to control rats. We observed an increase in sclerostin-positive osteocytes, which is consistent with the decreased ALP+area/BS and PHOSPHO1+area/BS values. These findings suggest that sclerostin, known to inhibit osteoblast activity [25], plays a role in suppressing bone formation in SDT-*fa/fa* rats. Sclerostin is predominantly developed by osteocytes and inhibits osteoblast differentiation and bone formation by antagonizing the canonical Wnt signaling pathway by binding lipoprotein receptor-related protein 5/6 to receptors with low-density lipoprotein [30-32]. Therefore, it seems likely that sclerostin derived from osteocytes diminishes osteoblastic activity in

SDT-*fa/fa* rats. If so, our finding in this study seems to be consistent with a previous report that elevated serum sclerostin concentrations were correlated with prevalent vertebral fractures in patients with T2DM irrespective of BMD and bone turnover factors [33]. Such results indicate that osteocyte dysfunction in patients with diabetes can lead to bone fragility, and our findings imply that diabetic osteoporosis not only affects osteoclasts and osteoblasts, the primary regulators of bone remodeling, but may also involve functional disruptions in the osteocyte network.

Another intriguing aspect was the accumulation of osteocalcin within the lacunae of SDT-*fa/fa* rats, which contrasts to its typical localization along bone surfaces and cement lines in control SD rats. In patients with T2DM, serum levels of osteocalcin, a marker of bone formation, are significantly reduced [33]. Additionally, markers of bone formation, PINP and OC, and markers of bone resorption CTX and TRAcP5b, are usually diminished in T2DM, whereas BSAP and NTX, markers of bone formation and resorption, respectively, are frequently normal or mildly elevated [34]. Kimura et al. [18] also reported decreased serum osteocalcin levels in 16-week-old SDT-*fa/fa* rats. While these findings reflect diminished osteoblast activity, the accumulation of osteocalcin in lacunae suggests that abnormalities in the osteocyte network, rather than changes in traditional bone remodeling processes, may be induced by diabetes.

Both DMP-1 and MEPE, proteins produced by osteocytes, were detected in the lacunae and canaliculi of control SD rats. However, in SDT-*fa/fa* rats, these proteins were confined to the lacunae, showing no significant immunoreactivity in the canaliculi. Interestingly, silver staining revealed no difference in the distribution of canaliculi between SD and SDT-*fa/fa* rats, suggesting that the aberrant distribution of DMP-1 and MEPE reflects a unique mechanism that causes their accumulation in lacunae. Our previous study on *kl/kl* mice discovered a similar trend, in which DMP-1 and osteocalcin accumulated in osteocyte lacunae, with electron microscopy revealing damage to these osteocytes despite the absence of visible abnormalities under light microscopy [24]. Although the bone environment in *kl/kl* mice differs significantly from that in SDT-*fa/fa* rats, hyperglycemia or increased lipoprotein levels may disrupt the osteocyte network in a similar manner, leading to protein accumulation in the lacunae.

Our current findings demonstrate that although the osteocyte-canalicular network is preserved in SDT-*fa/fa* rats, the localization of key osteocyte-derived proteins, such as sclerostin and osteocalcin, is altered. Further research is needed to determine the underlying mechanisms by which diabetes affects these changes and to explore the functional implications of osteocalcin accumulation within the lacunae.

Conclusions

Histochemical analysis of the femoral cancellous bone of 30-week-old male SDT-*fa/fa* rats revealed a reduction in trabecular bone and decreased BMD, primarily due to impaired bone formation by osteoblasts rather than enhanced bone resorption by osteoclasts. An increased number of sclerostin-positive osteocytes suggests that osteocytes may suppress osteoblast activity in diabetic osteoporosis. While no abnormalities were found in the distribution of the osteocyte-canalicular network, an accumulation of osteocalcin, DMP-1, and MEPE within lacunae indicates that the abnormal localization of these proteins may influence osteocyte function. Further studies are warranted to elucidate the mechanisms driving these alterations and their impact on bone health in diabetes.

Ethical standards

All animal experiments were performed in accordance with the Japanese Act on Welfare and Management of Animals. The protocol was approved by the Institutional Animal Care and Use Committee of Hokkaido University (approved research proposal #21-0013).

Competing interests

The authors declare no competing interests.

Contributors

Hasegawa T designed this study and prepared the final draft of the article. Yao Q was the first author in charge of writing the original draft and analyzing and interpreting the data. Tsuboi K, Hongo H, Sakakibara M, and Haraguchi-Kitakamae M contributed to the histochemical analysis. Yamamoto T, Ishizu H, Liu X, Shi Y, Li W, and Cui J worked on the statistical analyses. Shimizu T, Amizuka N, Yokoyama A, and Sakaguchi K participated in critically reading, editing, and formatting the manuscript.

References

1. Giri B, Dey S, Das T, Sarkar M, Banerjee J, Dash SK. Chronic hyperglycemia mediated physiological alteration and metabolic distortion leads to organ dysfunction, infection, cancer progression and other pathophysiological consequences: An update on glucose toxicity. *Biomed. Pharmacother.* 107:306–328, 2018.

2. Alberti KG, Zimmet PZ. Definition, diagnosis and classification of diabetes mellitus and its complications. Part 1: diagnosis and classification of diabetes mellitus provisional report of a WHO consultation. *Diabet Med.*15(7):539-553, 1998.

3. Napoli N, Chandran M, Pierroz DD, Abrahamsen B, Schwartz AV, Ferrari AL. Mechanisms of diabetes mellitus-induced bone fragility. *Nat Rev Endocrinol.* 13:208-219, 2017.

4. Hofbauer LC, Brueck CC, Singh SK, Dobnig H. Osteoporosis in patients with diabetes mellitus. *J Bone Miner Res.* 22(9):1317–1328, 2007.

5. Janghorbani M, Van Dam RM, Willett WC, Hu FB. Systematic review of type 1 and type 2 diabetes mellitus and risk of fracture. *Am J Epidemiol.* 66(5):495–505,2007.

6. Farr JN, Khosla S. Determinants of bone strength and quality in diabetes mellitus in humans. *Bone.* 82:28–34, 2016.

7. Krakauer JC, McKenna MJ, Buderer NF, Rao DS, Whitehouse FW, Parfitt AM. Bone loss and bone turnover in diabetes. *Diabetes.* 44(7):775–782, 1995.

8. Vestergaard P. Discrepancies in bone mineral density and fracture risk in patients with type 1 and type 2 diabetes—a meta-analysis. *Osteoporos Int.* 18(4):427–444, 2007.

9. Manavalan JS, Cremers S, Dempster DW, Zhou H, Dworakowski E, Kode A, et al. Circulating osteogenic precursor cells in type 2 diabetes mellitus. *J Clin Endocrinol Metab.* 97(9):3240–3250, 2012.

10. Ma L, Oei L, Jiang L, Estrada K, Chen H, Wang Z, et al. Association between bone mineral density and type 2 diabetes mellitus: a meta-analysis of observational studies. *European journal of epidemiology.* 27(5):319–332, 2012.

11. Poiana C, Capatina C. Osteoporosis and fracture risk in patients with type 2 diabetes mellitus. *Acta Endocrinol (Buc).* 15:231-236, 2019.

12. Starup-Linde J: Diabetes, biochemical markers of bone turnover, diabetes control, and bone. *Front Endocrinol.* 4:21, 2013.

13. Masuyama T, Katsuda Y, Shinohara M. A Novel Model of Obesity-Related Diabetes: Introgression of the *Lepr*^{fa} Allele of the Zucker Fatty Rat into Nonobese Spontaneously Diabetic Torii (SDT) rats. *Exp Anim.* 54(1):13–20, 2005.

14. Jensen T, Deckert T. Diabetic retinopathy, nephropathy and neuropathy. Generalized vascular damage in insulin-dependent diabetic patients. *Horm Metab Res Suppl.* 26:68–70, 1992.

15. Matsui K, Ohta T, Oda T, Sasase T, Ueda N, Miyajima K, et al. Diabetes-associated complications in spontaneously diabetic Torii fatty rats. *Exp Anim.* 57(2):111–121, 2008.

16. Matsui K, Ohta T, Oda T, Sasase T, Ueda N, Miyajima K, et al. Effects of preventing hyperphagia on glycolipid metabolic abnormalities in spontaneously diabetic Torii fatty rats. *Anim Sci J.* 79(5): 605–613, 2008.

17. Ishii Y, Maki M, Yamamoto H, Sasase T, Kakutani M, Ohta T. Evaluation of Blood Pressure in Spontaneously Diabetic Torii-*Lepr*^{fa} rats. *Exp Anim.* 59(4):525–529, 2010.

18. Kimura S, Sasase T, Ohta T, Sato E, MatsushitaM. Characteristics of bone turnover, bone mass and bone strength in Spontaneously Diabetic Torii-*Lepr*^{fa} rats. *J Bone Miner Metab.* 30(3): 312–320, 2012.

19. Ohta T, Kimura S, Hirata M, Yamada T, Sugiyama T. Bone morphological analyses in Spontaneously Diabetic Torii (SDT) fatty rats. *J Vet Med Sci.* 77(10):1327-1330, 2015.

20. Hasegawa T, Tokunaga S, Yamamoto T, Sakai M, Hongo H, Kawata T, et al. Evocalcet rescues secondary hyperparathyroidism-driven cortical porosity in CKD male rats. *Endocrinology*. 164(4):bqad022, 2023.

21. Hasegawa T, Yamamoto T, Sakai S, Miyamoto Y, Hongo H, Qiu Z, et al. Histological Effects of the Combined Administration of Eldecalcitol and a Parathyroid Hormone in the Metaphyseal Trabeculae of Ovariectomized Rats. *J Histochem Cytochem.* 67(3):169-184, 2019.

22. Oda K, Amaya Y, Fukushi-Irie M, Kinameri Y, Ohsuye K, Kubota I, et al. A general method for rapid purification of soluble versions of glycosylphosphatidylinositol-anchored proteins expressed in insect cells: An application for human tissue-nonspecific alkaline phosphatase. *J. Biochem.* 126(4):694–699, 1999.

23. Mae T, Hasegawa T, Hongo H, Yamamoto T, Zhao S, Li M, et al. Immunolocalization of enzymes/membrane transporters related to bone mineralization in the metaphyses of the long bones of parathyroid-hormone-administered mice. *Medicina*. 59(6):1179, 2023.

24. Sasaki M, Hasegawa T, Yamada T, Hongo H, de Freitas PH, Suzuki R, et al. Altered distribution of bone matrix proteins and defective bone mineralization in klotho-deficient mice. *Bone.* 57(1):206-219, 2013.

25. Hasegawa T, Amizuka N, Yamada T, Liu Z, Miyamoto Y, Y et al. Sclerostin is differently immunolocalized in metaphyseal trabecules and cortical bones of mouse tibiae. *Biomed Res.* 34(3):153-159, 2013.

26. Makino A, Hasegawa T, Yamamoto T, Takagi H, Takahashi Y, Miyakoshi N, et al. Abaloparatide promotes bone repair of vertebral defects in ovariectomized rats by increasing bone formation. *Bone.* 182:117056, 2024.

27. Hasegawa T, Yamamoto T, Hongo H, Yamamoto T, Haraguchi-Kitakamae M, Ishizu H, et al. Eldecalcitol Induces Minimodeling-Based Bone Formation and Inhibits Sclerostin Synthesis Preferentially in the Epiphyses Rather than the Metaphyses of the Long Bones in Rats. *Int J Mol Sci*. 25(8):4257, 2024.

28. Parfitt AM, Drezner MK, Glorieux FH, Kanis JA, Malluche H, et al. Bone histomorphometry: standardization of nomenclature, symbols, and units. Report of the ASBMR Histomorphometry Nomenclature Committee. *J Bone Miner Res.* 2(6):595–610, 1987.

29. Nomura S, Kitami A, Takao-Kawabata R, Takakura A, Nakatsugawa M, Kono R, et al. Teriparatide Improves Bone and Lipid Metabolism in a Male Rat Model of Type 2 Diabetes Mellitus. *Endocrinology,* 160(10):2339-2352, 2019.

30. Winkler DG, Sutherland MK, Geoghegan JC, Yu C, Hayes T, Skonier JE, et al. Osteocyte control of bone formation via sclerostin, a novel BMP antagonist. *EMBO J.* 22(23):6267-676, 2003.

31. Kusu N, Laurikkala J, Imanishi M, Usui H, Konishi M, Miyake A, et al. Sclerostin is a novel secreted osteoclast-derived bone morphogenetic protein antagonist with unique ligand specificity. *J Biol Chem.* 278(26):24113-24117, 2003.

32. Delgado-Calle J, Sato AY, Bellido T. Role and mechanism of action of sclerostin in bone. *Bone.* 96:29-37, 2017.

33. Kanazawa I, Sugimoto T. Diabetes mellitus-induced bone fragility . *Intern Med.* 57:2773-2785, 2018.

34. Ferrari SL, Abrahamsen B, Napoli N, Akesson K, Chandran M, Eastell R, et al. Diagnosis and management of bone fragility in diabetes: an emerging challenge. *Osteoporos Int.* 29(12):2585-2596, 2018.

	SD rats	SDT-*fa/fa* rats
GLU (mg/dl)	170.25 ± 19.24	675.17 ± 37.96 **
HbA1c (%)	5.01 ± 0.08	9.94 ± 0.36 **
T-CHO (mg/dl)	71.50 ± 4.09	162.83 ± 21.56 *
TG (mg/dl)	55.00 ± 24.84	414.83 ± 60.08 *
HDL-C (mg/dl)	23.25 ± 2.06	50.67 ± 3.52 **
CRE(mg/dl)	0.38 ± 0.04	0.28 ± 0.03
BUN(mg/dl)	19.95 ± 0.92	28.65 ± 2.91 *
Ca(mg/dl)	9.98 ± 0.53	9.93 ± 0.34
iP(mg/dl)	8.03 ± 1.72	7.70 ± 0.94
Na (mEq/L)	143.25 ±1.80	134.67 ± 1.45 *
K (mEq/L)	4.68 ± 0.38	5.57 ± 0.37

Table 1

Means ± SD and statistical analysis results for serum and urea markers in Sprague–Dawley (SD) and Spontaneously Diabetic Torii fatty (SDT-*fa/fa*) rats

All statistical differences between meansa were assessed by Student's *t*-tests. Values of $P < 0.05$ were considered significant: ** indicates $P < 0.001$ and * indicates $P < 0.01$.

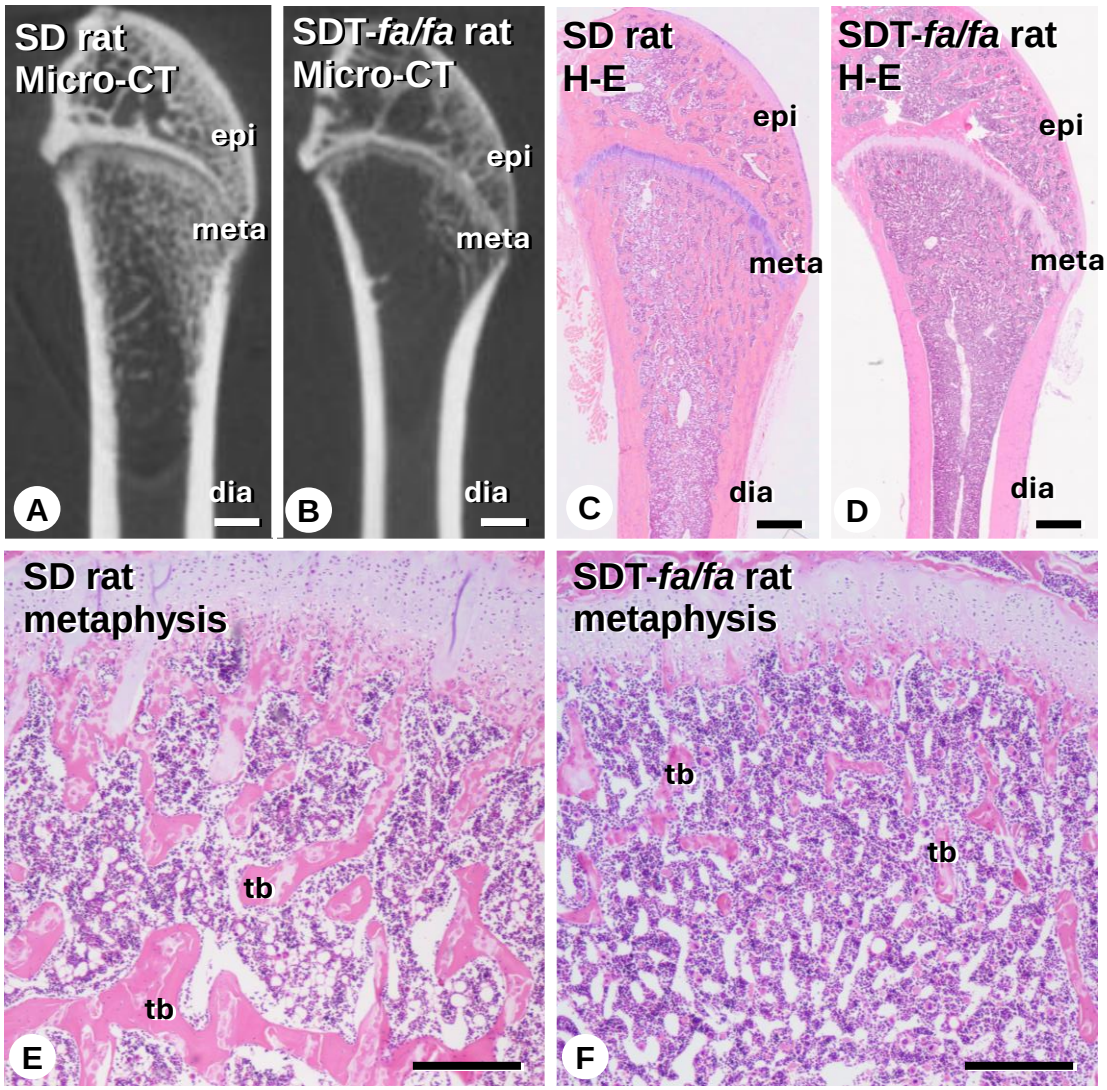
SD rat
Micro-CT
epi
meta
dia
A
SDT-fa/fa rat
Micro-CT
epi
meta
dia
B
SD rat
H-E
epi
meta
dia
C
SDT-fa/fa rat
H-E
epi
meta
dia
D
SD rat
metaphysis
tb
tb
E
SDT-fa/fa rat
metaphysis
tb
tb
F

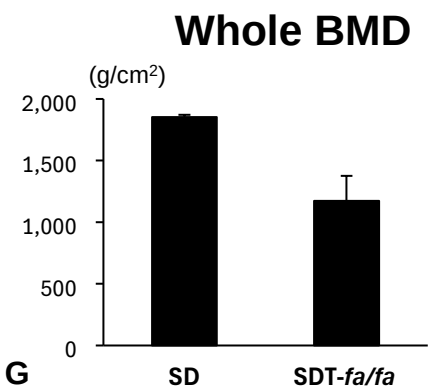
Whole BMD
(g/cm²)
2,000
1,500
1,000
500
0
SD
SDT-fa/fa
G

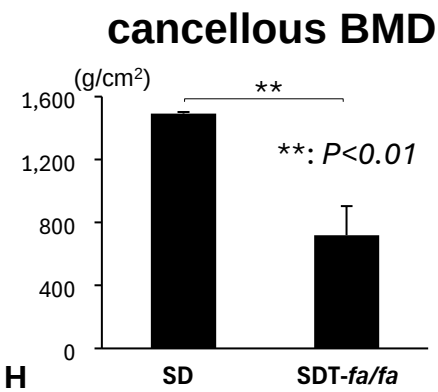
cancellous BMD
(g/cm²)
1,600
1,200
800
400
0
**
**: P<0.01
SD
SDT-fa/fa
H

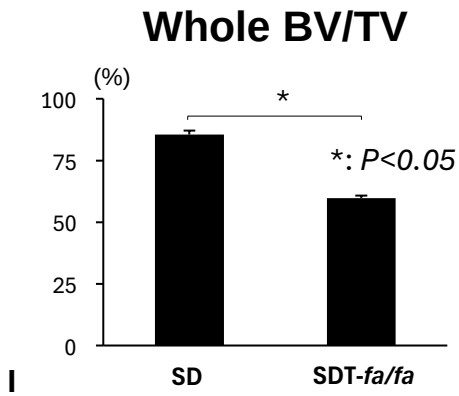
Whole BV/TV
(%)
100
75
50
25
0
*
*: P<0.05
SD
SDT-fa/fa
I

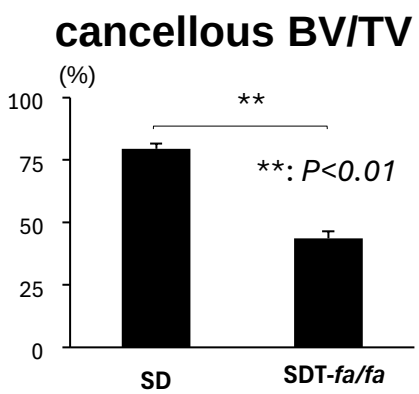
cancellous BV/TV
(%)
100
75
50
25
0
**
**: P<0.01
SD
SDT-fa/fa
J

Figure 1

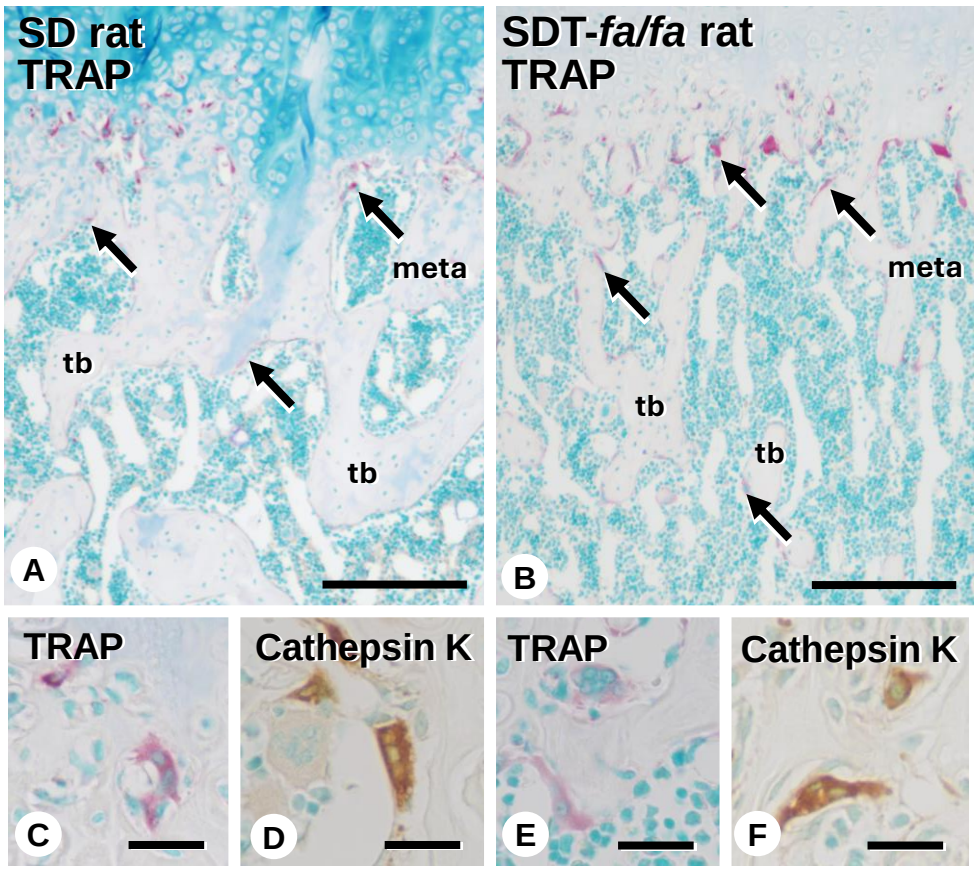
SD rat
TRAP
meta
tb
tb
A
SDT-fa/fa rat
TRAP
meta
tb
tb
B
TRAP
C
Cathepsin K
D
TRAP
E
Cathepsin K
F

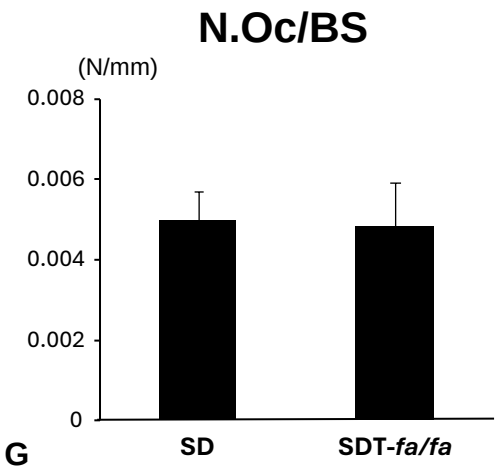
N.Oc/BS
(N/mm)
0.008
0.006
0.004
0.002
0
SD
SDT-fa/fa
G

Figure 2

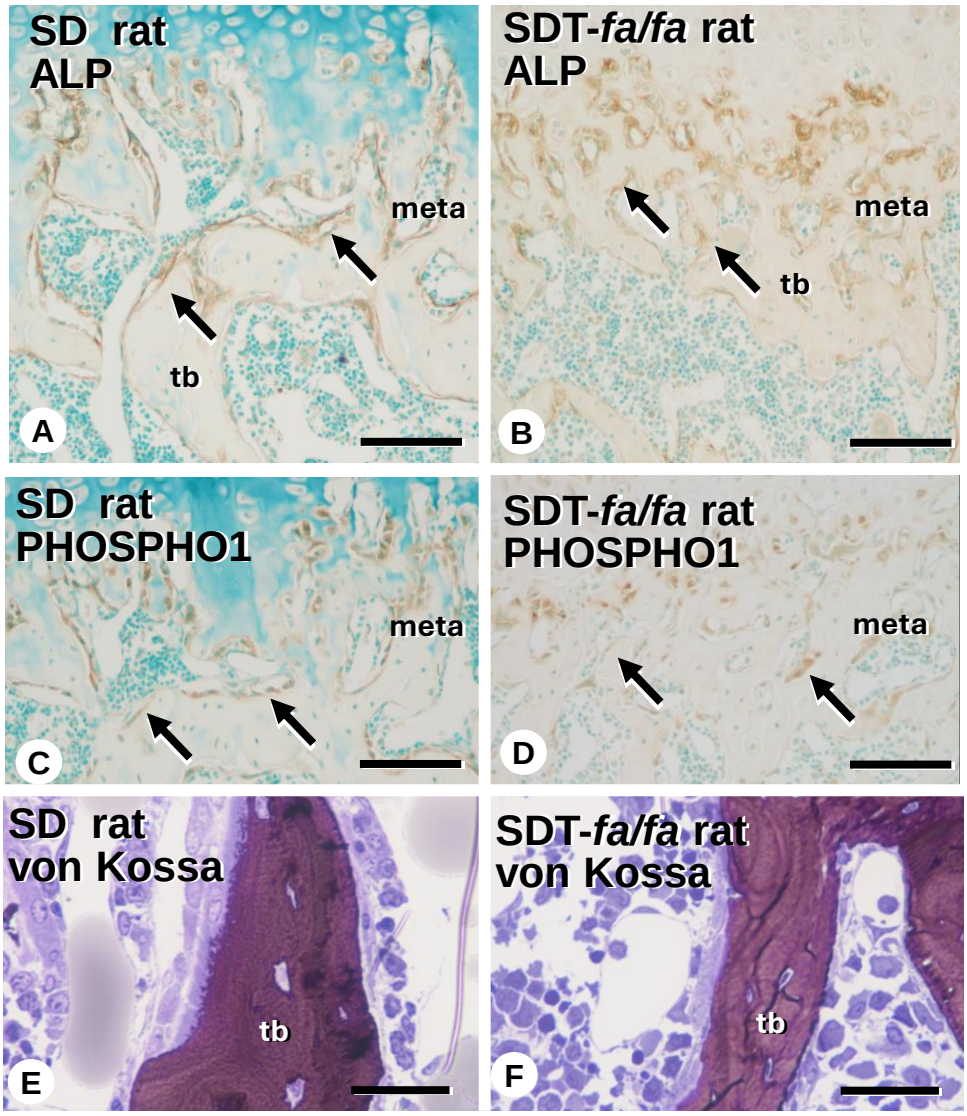
SD rat
ALP
meta
tb
A
SDT-fa/fa rat
ALP
meta
tb
B
SD rat
PHOSPHO1
meta
C
SDT-fa/fa rat
PHOSPHO1
meta
D
SD rat
von Kossa
tb
E
SDT-fa/fa rat
von Kossa
tb
F

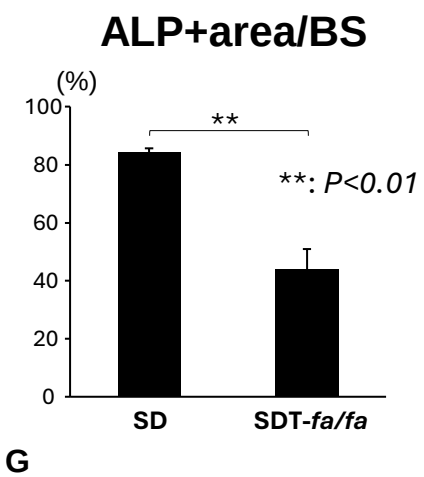
ALP+area/BS
(%)
100
80
60
40
20
0
**
**: P<0.01
SD
SDT-fa/fa

G

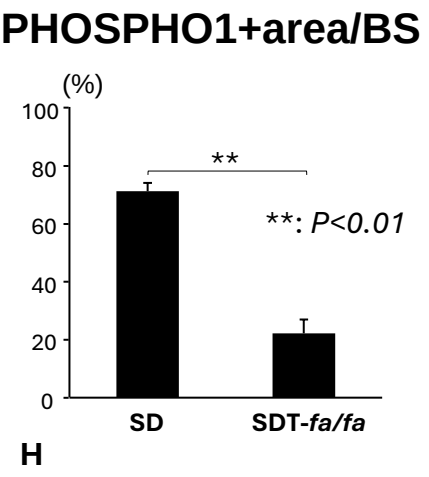
PHOSPHO1+area/BS
(%)
100
80
60
40
20
0
**
**: P<0.01
SD
SDT-fa/fa

H

Figure 3

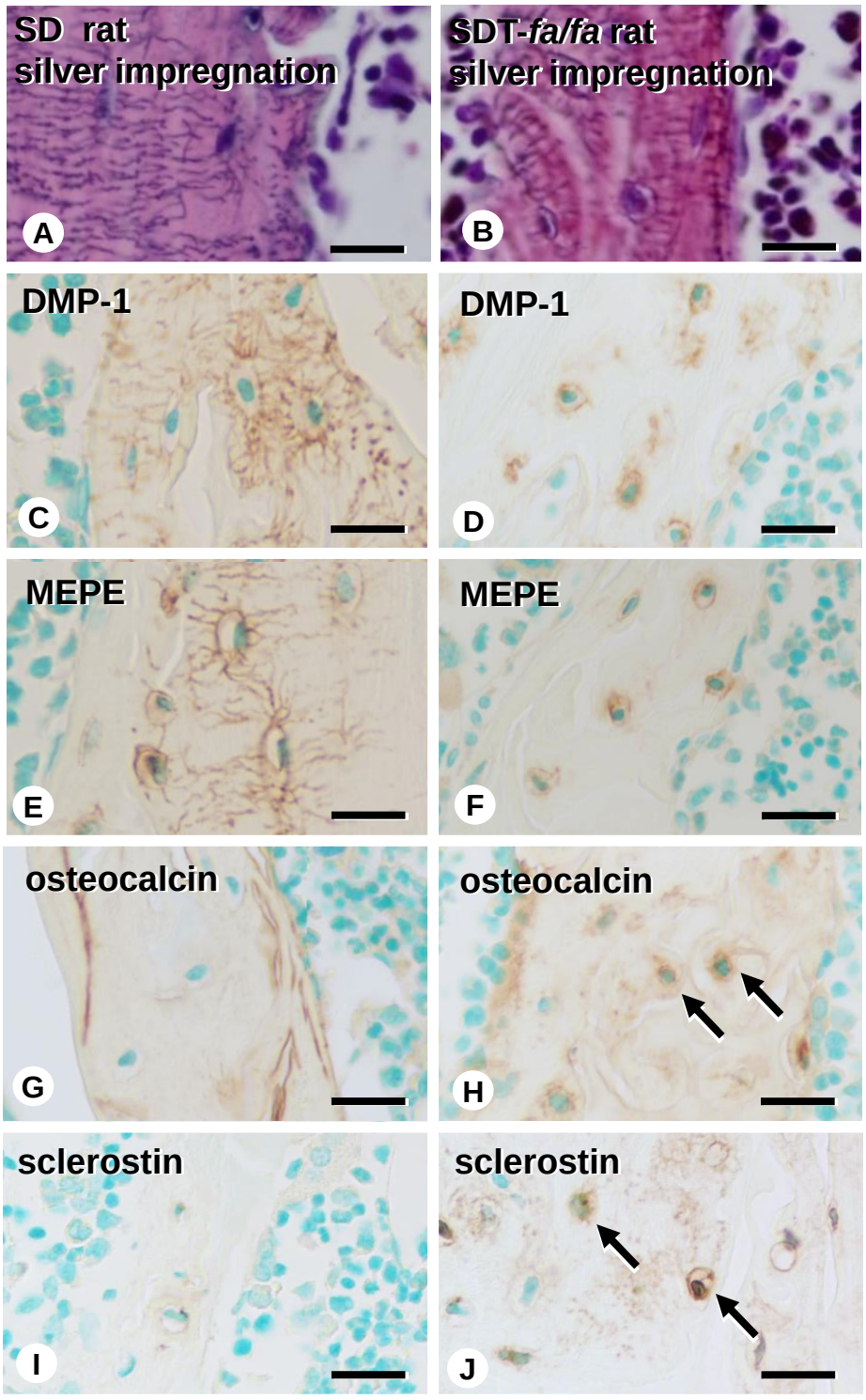
SD rat
silver impregnation
A
SDT-fa/fa rat
silver impregnation
B
DMP-1
C
DMP-1
D
MEPE
E
MEPE
F
osteocalcin
G
osteocalcin
H
sclerostin
I
sclerostin
J

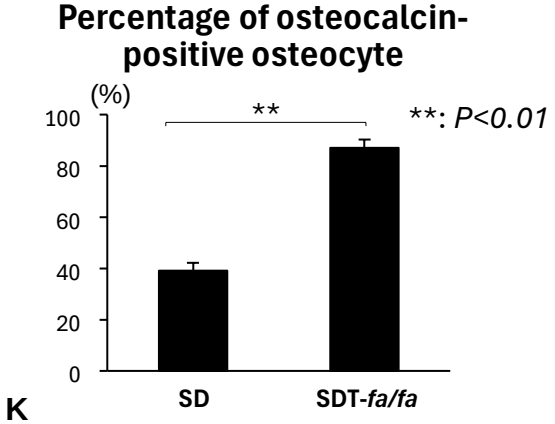
Percentage of osteocalcin-positive osteocyte
(%)
100
80
60
40
20
0
**
**: P<0.01
SD
SDT-fa/fa
K

Figure 4

Figure Legends

Figure 1

Micro-CT and histological images of femora in SD and SDT-fa/fa rats

Panels **A**–**D** show micro-CT **(A, B)** and histological **(C, D)** images of the femoral distal region of SD **(A, C)** and SDT-*fa/fa* **(B, D)** rats. Panels **E** and **F** are high-magnification images of the femoral metaphyses of SD **(E)** and SDT-*fa/fa* **(F)** rats. Note the lower numbers of metaphyseal trabeculae in SDT-*fa/fa* femora **(B, D, F)** in comparison with SD femora **(A, C, E)**. Panels **G** and **H** are bar graphs representing whole BMD and cancellous BMD, respectively. Panels **I** and **J** show whole BV/TV and cancellous bone, respectively. All values are presented as means ± SD (*: $P < 0.05$, **: $P < 0.01$). epi: epiphysis, meta: metaphysis, dia: diaphysis, tb: trabecular bone

Bars, A–D: 1000μm, E, F: 300μm

Figure 2

Osteoclast distribution in the femora of SD and SDT-fa/fa rats

Panels **A** and **B** are low-magnified images of femoral metaphyses showing the distribution of TRAP-positive osteoclasts (red color) in SD and SDT-*fa/fa* rats, respectively. When observing TRAP-positive (red color, **C, E**) and cathepsin K-reactive (brown color, **D, F**) osteoclasts at a higher magnification, the patterns and intensities of TRAP **(C, E)** and immunoreactivity of cathepsin K **(D, F)** are similar between the SD **(C, D)** and SDT-*fa/fa* **(E, F)** rats. The graph in panel **G** represents the mean N.Oc/BS values (± SD) in the ROIs of SD and SDT-*fa/fa* rats. Note that no significant difference was found between the two rats. meta: metaphysis, tb: trabecular bone

Bars, A, B: 200μm, C–F: 30μm

Figure 3

Osteoblast distribution in the femora of SD and SDT-fa/fa rats

Panels **A**–**D** are images showing ALP-immunostaining (brown color, **A, B**) and PHOSPHO1 immunodetection (brown color, **C, D**) in the femoral metaphyses of SD **(A, C)** and SDT-*fa/fa* **(B, D)** rats. Panels **E** and **F** are images of von Kossa-stained femoral metaphyses visualizing bone mineralization (brown color). Bar graphs **G** and **H** show the means ± SD and statistical analysis results for ALP+area/BS and PHOSPHO1+area/BS, respectively, in the SD and SDT-*fa/fa* rats. Note the significantly reduced ALP+area/BS and PHOSPHO1+area/BS in SDT-*fa/fa* rats. $^{**}P<0.01$, $^{***}P<0.001$ meta: metaphysis, tb: trabecular bone

Bars, A–B: 100μm, E, F: 30μm

Figure 4

Osteocyte-derived peptides distribution in SD and SDT-fa/fa rats

Panels **A** and **B** show silver-impregnated metaphyseal trabeculae of SD and SDT-*fa/fa* rats, respectively, visualizing osteocytic lacunae and canaliculi within the trabecular structure. Panels **C**–**J** show immunostaining for DMP-1 **(C, D)**, MEPE **(E, F)**, osteocalcin **(G, H),** and sclerostin **(I, J)** in the metaphyseal trabeculae of SD **(C, E, G, I)** and SDT-*fa/fa* **(D, F, H, J)** rats. Note that there is only a faint immunoreactivity of DMP-1 and MEPE in the osteocytic canaliculi in the SDT-*fa/fa* rats **(D, F)** and that this immunoreactivity is much more intense in the SD rats **(C, E)**. Also, note the intense immunoreactivity of osteocalcin and sclerostin in the osteocytic lacunae of SDT-*fa/fa* rats **(arrows, H, J)**, which is much fainter in the SD rats **(G, I)**. Panel **K** is a graph representing the mean percentage (± SD) of osteocalcin-immunopositive osteocytes in the SD and SDT-*fa/fa* rats. $^{**}P<0.01$

Bars, A–J: 30μm